The Astrophysical Journal, 941:118 (11pp), 2022 December 20 https://doi.org/10.3847/1538-4357/aca1ad

The Small Separation A-star Companion Population: First Results with CHARA/MIRC-X

Matthew De Furio[1], Tyler Gardner[2], John Monnier[1], Michael R. Meyer[1], Kaitlin Kratter[3], Gail Schaefer[4], Narsireddy Anugu[3,4], Claire L. Davies[2], Stefan Kraus[2], Cyprien Lanthermann[4], Jean-Baptiste Le Bouquin[5], and Jacob Ennis[1]

[1] Department of Astronomy, University of Michigan, Ann Arbor, MI, USA; defurio@umich.edu
[2] Astrophysics Group, Department of Physics and Astronomy, University of Exeter, Stocker Road, Exeter, EX4 4QL, UK
[3] Department of Astronomy and Steward Observatory, University of Arizona, Tucson, AZ, USA
[4] CHARA Array, Georgia State University, Atlanta, GA 30302, USA
[5] Université Grenoble Alpes, CNRS, IPAG, F-38000, Grenoble, France
Received 2022 February 26; revised 2022 October 14; accepted 2022 November 2; published 2022 December 15

Abstract

We present preliminary results from our long-baseline interferometry (LBI) survey to constrain the multiplicity properties of intermediate-mass A-type stars within 80 pc. Previous multiplicity studies of nearby stars exhibit orbital separation distributions well fitted with a lognormal with peaks >15 au, increasing with primary mass. The A-star multiplicity survey of De Rosa et al., sensitive beyond 30 au but incomplete below 100 au, found a lognormal peak around 390 au. Radial velocity surveys of slowly rotating, chemically peculiar Am stars identified a significant number of very close companions with periods ⩽5 days, ∼0.1 au, a result similar to surveys of O- and B-type primaries. With the improved performance of LBI techniques, we can probe these close separations for normal A-type stars where other surveys are incomplete. Our initial sample consists of 27 A-type primaries with estimated masses between 1.44 and 2.49 $M_{\odot}$ and ages 10–790 Myr, which we observed with the MIRC-X instrument at the CHARA Array. We use the open-source software CANDID to detect five companions, three of which are new, and derive a companion frequency of $0.19^{+0.11}_{-0.06}$ over mass ratios of 0.25–1.0 and projected separations of 0.288–5.481 au. We find a probability of 10^{-6} that our results are consistent with extrapolations based on previous models of the A-star companion population over the mass ratios and separations sampled. Our results show the need to explore these very close separations to inform our understanding of stellar formation and evolution processes.

Unified Astronomy Thesaurus concepts: Intermediate-type stars (818); Multiple stars (1081); Binary stars (154); Star formation (1569); Long baseline interferometry (932); Close binary stars (254); Stellar types (1634); Chemically peculiar stars (226)

Supporting material: tar.gz file

1. Introduction

Multiplicity is a common outcome of the star formation process, the properties of which, e.g., orbital separation and mass ratio, seemingly depend on the primary mass of the system (Duchene & Kraus 2013; Moe & Di Stefano 2017). Multiple systems tend to form through two common processes: disk fragmentation (Adams et al. 1989; Bonnell & Bate 1994; Kratter et al. 2008) and turbulent fragmentation (Goodwin et al. 2004; Offner et al. 2010). Disk fragmentation is thought to account for the origin of companions at separations on the order of the size of the disk (tens to hundreds of au), while turbulent fragmentation is thought to account for the origin of companions at wider separations (tens to hundreds of au). Close companions (0.1–10 au) are found around various types of stars regardless of mass (e.g., Reid et al. 2006; Raghavan et al. 2010; Sana et al. 2012), but additional processes are needed to explain their separations. Orbits can shrink, even for initially wide binaries, through interactions between the companion and infalling gas from the natal cloud, direct interactions with a circumstellar disk, and dynamical interactions of unstable multiple systems (Bate et al. 2002, 2003; Offner et al. 2010; Bate 2012). These small separation companions have significant impacts on our fundamental understanding of planet formation and stellar evolution, as well as star formation.

Many volume-limited surveys have characterized the stellar multiple population based on primary star mass, mass ratio, and orbital separation. They found that the companion orbital separation distribution can be fitted as a lognormal distribution with a peak >15 au that increases with primary mass. Low-mass M-type primaries have a companion separation peak around 20 au (Janson et al. 2012; Winters et al. 2019), solar-type primaries have a peak at 50 au (Raghavan et al. 2010), and A-type primaries have a peak around 390 au (De Rosa et al. 2014). However, the A-type multiplicity survey of De Rosa et al. (2014) is incomplete for separations <100 au, leaving open the possibility for a significant population of close separation companions to A-type primaries.

Radial velocity surveys of chemically peculiar Am stars with small rotational velocities identified a significant number of very close companions with a characteristic period of 5 days, ∼0.1 au (Abt & Levy 1985; Carquillat & Prieur 2007). Close companions could drive the decreased rotational velocity and thus the peculiar chemical composition of Am stars. But a similar peak has been identified for O-type primaries (Sana et al. 2012). Interferometric

studies of OB primaries in the Orion Nebula Cluster found a bimodal distribution with peaks at ∼1 and 400–600 au (Gravity Collaboration et al. 2018). A similar population of close companions to normal A stars would be vitally important to understanding possible planetary architectures around intermediate-mass stars and the formation mechanisms required to form small separation binaries as a function of primary mass.

If small separation companions to intermediate-mass stars are common, they could represent a likely formation mechanism of Type Ia supernova progenitors, i.e., white dwarfs with masses $\geqslant 0.7\ M_{\odot}$ evolved from intermediate-mass stars (Cummings et al. 2018). One such binary with a high mass ratio could result in the double-degenerate scenario, where two white dwarfs with masses of ∼0.7–0.8 $M_{\odot}$ form and eventually merge, producing a Type Ia supernova as the combined mass exceeds the Chandrashekhar mass limit (Webbink 1984). These types of multiples could also produce the single-degenerate scenario, where a white dwarf accretes hydrogen from a close companion star and eventually detonates when surpassing the Chandrashekhar mass limit (Whelan & Iben 1973).

Identifying close companions to A stars with the radial velocity method can be more difficult than for solar-type stars, as their spectral lines are quite broad due to their fast rotation (Borgniet et al. 2019). Radial velocity surveys also require frequent observations over multiple years to detect companions at several au in separation for a typical A-type star. Extreme adaptive optics (AO) systems can achieve angular resolutions down to ∼20 mas but cannot resolve the region in which Am stars have close companions (∼0.1 au) at distances >5 pc. Therefore, we used the Michigan Infra-Red Combiner-eXeter (MIRC-X) instrument (Anugu et al. 2020) on the long-baseline interferometric array at the Center for High Angular Resolution Astronomy (CHARA; ten Brummelaar et al. 2005) to observe a pilot sample of A-type stars within 80 pc and search for close companions down to separations of 0.5 mas.

In Section 2, we describe the data and the methods to identify companions. In Section 3, we present the companion detections, describe our detection limits, and make a preliminary estimate of the close companion population of A-type primary stars. In Section 4, we compare our results to various multiplicity surveys and discuss the implications. In Section 5, we summarize our conclusions.

2. Methods

2.1. Observations

We observed 26 A-type stars over the course of 2 nights (UT 2020 December 20–21) at the CHARA Array with the MIRC-X instrument in the near-infrared H photometric band (∼1.6 μm), listed in Table 1. The CHARA Array is an interferometer made up of six 1 m telescopes that operate in the optical and near-infrared with baselines ranging from 34 to 331 m. The MIRC-X is a beam combiner instrument (Monnier et al. 2006; Anugu et al. 2020) that operates in the near-infrared using all CHARA telescopes. All of our observations were taken in the grism mode with $R \sim 190$. This spectral mode allows us to search out to wide angular scales (∼0.″3), as the increased spectral dispersion increases the interferometric field of view (Anugu et al. 2020). At the same time, the spectral resolution is not so high that flux is spread out across many spectral channels, reducing the signal-to-noise ratio (S/N) and thus the achievable contrast. The R190 grism is ideal for observing our relatively bright targets (typically $H =$ 4–5.5 mag) and searching for companions on wide angular scales. One other target (HD 31647) was observed on UT 2021 October 21 with a five-telescope setup (missing telescope W2) using both MIRC-X (R190) and MYSTIC (prism, R50; Monnier et al. 2018), a beam combiner in the same vein as MIRC-X that operates in the K band (∼2.2 μm), making our sample size a total of 27.

For each target, we had the same observing sequence: 10 minutes of source integration, the standard shutter sequence (Anugu et al. 2020), and a repeated 10 minutes of source integration. For HD 56537, we performed 5 minute source integrations instead due to the high flux of the primary to achieve an equivalent S/N to all other targets. Throughout our run, we observed calibrator stars for every few targets using an observing sequence of 5–10 minute integrations, shutters, and 5–10 minute integrations. Two of our calibrators (HD 15734 and HD 78234) are resolved binaries, and instead, we opted to use science targets well fit by a single star model to calibrate other targets observed in proximity; see Table 2. We opted to observe more science targets instead of more frequent calibrators because our search for companions relies on closure

Table 1
Table of Sources in Our Sample with Modified Julian Date of Observation

Target Name	Sp. Type	Distance (pc)	Age (Myr)	Mass ($M_{\odot}$)	MJD
HD 5448	A5V	$42.37^{+0.11}_{-0.19}$	450	2.39	59,203.08
HD 11636[b]	A5V	$18.27^{+0.25}_{-0.25}$	630	2.01	59,204.08
HD 15550	A9V	$71.77^{+1.84}_{-0.56}$	790	1.84	59,204.14
HD 20677	A3V	$48.11^{+0.30}_{-0.25}$	250	2.11	59,203.18
HD 21912	A3V	$56.29^{+0.16}_{-0.15}$	40	1.77	59,203.16
HD 24809	A8V	$63.76^{+0.12}_{-0.11}$	100	1.7	59,203.22
HD 28910	A8V	$46.97^{+0.38}_{-0.37}$	630	2.21	59,204.22
HD 29388[b]	A6V	$47.1^{+1.2}_{-1.2}$	630	2.17	59,204.19
HD 31647[a]	A1V	$49.91^{+0.29}_{-0.29}$	30	2.39	59,508.56
HD 32301	A7V	$57.55^{+4.80}_{-1.87}$	630	2.22	59,204.25
HD 46089[b]	A3V	$63.7^{+1.5}_{-1.5}$	560	2.20	59,203.29
HD 48097[b]	A2V	$43.6^{+1.3}_{-1.3}$	30	1.94	59,203.32
HD 56537[b]	A3V	$30.9^{+0.2}_{-0.2}$	320	2.39	59,204.28
HD 59037	A4V	$55.91^{+3.84}_{-1.44}$	500	2.16	59,203.35
HD 66664	A1V	$65.89^{+0.70}_{-0.58}$	320	2.42	59,204.33
HD 74198[b]	A1IV	$55.6^{+0.6}_{-0.6}$	320	2.49	59,204.39
HD 74873	A1V	$54.82^{+0.15}_{-0.14}$	50	1.88	59,204.36
HD 77660	A8V	$78.28^{+0.20}_{-0.19}$	710	1.81	59,203.43
HD 84107	A2IV	$51.24^{+2.38}_{-0.98}$	10	1.44	59,203.45
HD 92941[b]	A5V	$66.9^{+1.4}_{-1.4}$	450	1.84	59,204.48
HD 97244	A5V	$62.19^{+0.18}_{-0.15}$	60	1.72	59,204.45
HD 99787	A2V	$69.64^{+0.68}_{-0.89}$	280	2.32	59,203.48
HD 106661	A3V	$66.01^{+0.09}_{-0.21}$	400	2.29	59,204.51
HD 112734	A5	$73.73^{+0.44}_{-0.30}$	40	1.69	59,203.53
HD 115271[b]	A7V	$74.1^{+2.4}_{-2.4}$	560	2.10	59,203.59
HD 120047	A5V	$52.84^{+0.79}_{-0.39}$	500	1.78	59,204.60
HD 121164	A7V	$73.60^{+0.58}_{-0.44}$	500	1.97	59,204.57

Notes. Listed spectral types, ages, and masses for each star were taken from De Rosa et al. (2014), who described their method of estimating age and mass in their Appendix. Distances and their errors (16% and 84% confidence level) were extracted from the Gaia DR3 archive (Gaia Collaboration et al. 2016; Babusiaux et al. 2022; Gaia Collaboration et al. 2022), except where noted.
[a] Observed with both MIRC-X and MYSTIC at the CHARA Array.
[b] Distance taken from De Rosa et al. (2014) using the Hipparcos catalog (Hip 1997).

Table 2
Table of Calibrators

Calibrator Name	UD Diameter (mas)	Night UT	UD Reference
HD 99787	0.303 ± 0.024	2020 Dec 20	1
HD 44851	0.58 ± 0.014	2020 Dec 20	2
HD 21912	0.276 ± 0.007	2020 Dec 20	2
HD 120047	0.308 ± 0.008	2020 Dec 21	2
HD 32301	0.479 ± 0.033	2020 Dec 21	2
HD 74198	0.362 ± 0.024	2020 Dec 21	2
HD 19066[a]	0.85 ± 0.06	2021 Oct 21	2

Note.
[a] Observed with both MIRC-X and MYSTIC at the CHARA Array.
References. (1) Swihart et al. (2017); (2) Bourges et al. (2017).

phases and does not need highly calibrated visibilities; see Section 2.3.

2.2. Data Reduction

We used the standard MIRC-X data pipeline (version 1.3.3) to produce OIFITS files for each night, described in Anugu et al. (2020). The MIRC-X pipeline and its documentation is maintained on Gitlab.[6] This pipeline measures the visibilities, closure phases, and differential phases from each baseline pair in the raw interferometric data. We reduced our data with most of the default reduction parameters, setting the number of coherent integration frames to 10. We used an OIFITS maximum integration time of 60 s, which is lower than the default value of 150 s. This allows us to search for wider binaries, which create signals in visibility and phase that vary on faster timescales.

To calibrate the data and produce our final OIFITS files, we used a modified version of the MIRC-X pipeline, which uses similar routines in IDL as the pipeline for the previous Michigan InfraRed Combiner (MIRC; Monnier et al. 2007; Zhao et al. 2009; Che et al. 2011; Monnier et al. 2012). This routine is well tested with previous MIRC data to properly flag and remove bad data, which can otherwise corrupt binary fits and lead to worse nondetection maps. The reduced OIFITS files of each source within our sample are available in a .tar.gz package for download with this publication or on the CHARA data reduction machine,[7] which is open to the public upon request for an account.

2.3. Data Analysis

In order to identify companions to the targets in our sample of A-type stars, we applied the open-source python code Companion Analysis and Non-Detection in Interferometric Data (CANDID; Gallenne et al. 2015) to the OIFITS data of each observation. This code is designed to identify companions through a grid search of three-dimensional space (position and flux ratio). It can use information from the visibilities, bispectrum amplitudes, and/or closure phases to perform binary model fitting for a given data set. Closure phase is an interferometric quantity derived from the fringe phases of each pair of apertures within a closed triangle of three baselines (e.g., three telescopes) utilized to remove phase errors (Jennison 1958; Rogers et al. 1974; Monnier 2000; Monnier et al. 2004). For our purposes, we only used the closure phase information to find companions.

A symmetric brightness distribution will have measured closure phases of 0° or 180° within the errors of the measurements for each combination of three telescopes. Any scene deviating from a point-symmetric object (e.g., a binary) will produce nonzero closure phases with amplitudes on the order of the amount of deviation (e.g., flux ratio). In this case, the grid search of CANDID will find the best-fit binary model that best replicates the observed closure phases, including those deviating from zero.

CANDID provides a figure of merit in terms of $n\sigma$ calculated from χ^2 statistics, defined in Gallenne et al. (2015), to differentiate between a single source (uniform disk) and a binary model from the searched grid space. First, we used the closure phase and visibility information to best estimate the diameter of the primary star with CANDID, which we then used as the diameter of the uniform disk model. We then searched for companions within the closure phase data out to separations of $0\farcs3$, the extent of the interferometric field of view in grism mode. We define 5σ as the cutoff for companion detection as suggested by the CANDID authors.

Upon detection of a companion, we rerun CANDID using all available variables to derive the best-fit binary model to the closure phase and visibility data. CANDID allows for the fitting of the diameter of both components of the binary, as well as fitting the "resolved flux" value, which represents the visibility at a baseline of zero, typically accounting for any errors in calibration. For binaries where we can resolve both components, our final binary model has six parameters: separation and position angle of the companion relative to the primary, the diameters of each component, the flux ratio between components, and the resolved flux of the visibility data. For binaries with only a resolvable primary, we assume a diameter of 0.01 mas for the companion and use a five-parameter binary model. See Table 3 showing the values of each of these parameters for our detections.

3. Results

3.1. Detections

We detected five companions out of the 27 A-type stars in our sample. All detections had a significance of 8σ, the maximum permitted value in CANDID, indicative of strong detections. These companions were detected at projected separations = 6–65 mas (physical separation = 0.288–2.760 au) with flux ratios = 1.5%–80%; see Figure 1 and Table 3. Two of these detections, HD 11636 and HD 28910, were previously reported as spectroscopic binaries (Abt 1965; Pourbaix 2000), with only HD 11636 having reliable orbital parameters. Based on the inclination, eccentricity, and semimajor axis estimates of Pourbaix (2000), we estimate the range of possible projected separations for HD 11636 to be from 4 to 68 mas, consistent with our detection at 64 mas near apocenter. All five targets for which we detected a companion (except HD 11636, too bright for reliable Gaia information) were reported as having a proper-motion anomaly using Hipparcos and Gaia catalogs that could be indicative of a companion (Kervella et al. 2019). However, only one of the five detections we made (HD 28910) was identified in Gaia Data Release 3 (DR3) as a nonsingle star (Gaia Collaboration et al. 2022). Gaia DR3

[6] https://gitlab.chara.gsu.edu/lebouquj/mircx_pipeline; remember to include the underscore in copied link.
[7] https://www.chara.gsu.edu/observers/database

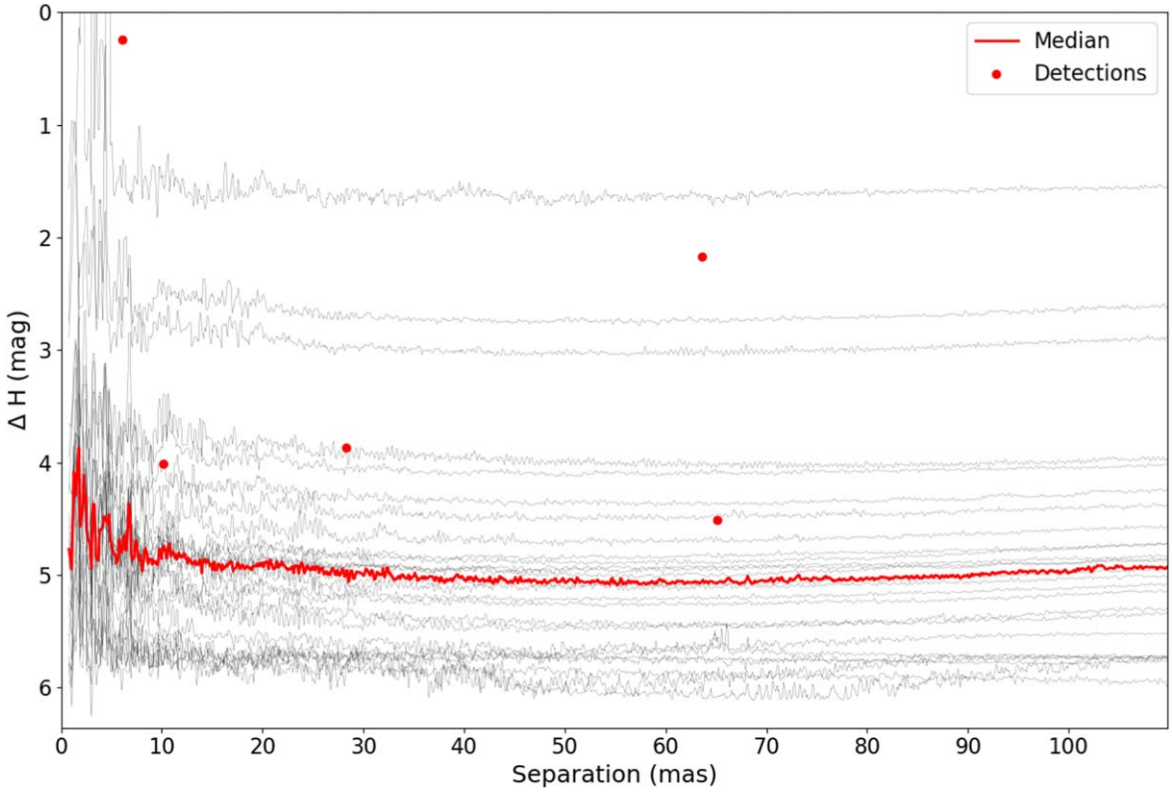

Figure 1. The detection limits derived from CANDID for each source are plotted in black, with the median value at each separation displayed in red. Detection limits correspond to the highest companion flux at a given separation over all position angles that results in a 5σ detection. Red circles represent the detections made in our survey at their given separation and contrast.

Table 3
Fitted Binary Parameters to Detected Binaries

Target Name (1)	Resolved Flux (% Primary) (2)	Flux Ratio (% Primary) (3)	Projected Sep. (mas) (4)	PA (deg) (E of N) (5)	UD_1 (mas) (6)	UD_2 (mas) 7	$\chi^2_{\nu,1}$ (8)	$\chi^2_{\nu,2}$ (9)
HD 5448	$-3.61^{+0.64}_{-0.70}$	$1.573^{+0.039}_{-0.042}$	65.132 ± 0.007	144.324 ± 0.007	0.695 ± 0.002	⋯	1.75	1.22
HD 11636	$1.97^{+0.34}_{-0.38}$	$13.546^{+0.11}_{-0.089}$	63.632 ± 0.002	102.271 ± 0.002	1.0819 ± 0.0008	0.549 ± 0.007	159.5	3.18
HD 28910	$4.09^{+0.72}_{-0.87}$	$80.146^{+0.064}_{-0.067}$	6.135 ± 0.0013	304.81 ± 0.012	$0.377^{+0.007}_{-0.006}$	$0.341^{+0.008}_{-0.007}$	1332	1.17
HD 29388	$1.535^{+0.29}_{-0.32}$	$2.488^{+0.024}_{-0.023}$	10.180 ± 0.002	23.59 ± 0.02	0.553 ± 0.005	⋯	4.39	1.14
HD 48097	$7.25^{+0.69}_{-0.66}$	$2.84^{+0.119}_{-0.11}$	28.296 ± 0.007	14.16 ± 0.02	0.288 ± 0.015	⋯	2.26	1.51

Note. Detected binaries with resolved flux and flux ratio in percent relative to the primary, projected separations in arcseconds, position angles in degrees, uniform disk diameter of the primary and secondary in milliarcseconds, and the reduced $\chi 2$ test statistic of a single and binary star model. All parameters were derived using CANDID fitting to the closure phase and visibility data. All detections achieved the maximum significance threshold on CANDID, 8σ.

reports a period of 58.94 ± 0.09 days and an eccentricity of 0.31 ± 0.16. Given our mass estimate of this system (see Table 4) and the period from Gaia, we estimate a semimajor axis of 0.48 au and a minimum and maximum distance from the primary of 0.33 and 0.63 au assuming the eccentricity from Gaia. Our estimate of 0.288 au is within the errors of the current Gaia estimate, indicative of a larger eccentricity than the median Gaia value. Only one other source in our sample was identified in Gaia DR3 as being a nonsingle star, HD 21912, which has a spectroscopically identified companion with a period of 0.92 days (Gaia Collaboration et al. 2022), likely at a separation smaller than our sensitivity. All other sources within our sample had no companion detections in either our analysis or Gaia DR3.

Because the estimated ages of our targets range from 10 to 790 Myr (see Table 1), we estimated the masses of each companion using the MIST evolutionary models (Paxton et al. 2011, 2013, 2015; Choi et al. 2016; Dotter 2016; Paxton et al. 2018). We assumed the primary mass and age estimates from De Rosa et al. (2014). They estimated ages based on the source position on the color–magnitude diagram relative to theoretical isochrones, and they estimated masses based on their 2MASS K-band magnitude and estimated ages. We adopt these values for the primary stars and use the MIST isochrones to determine companion masses from the magnitude differences derived in CANDID. The mass ratios (q) of the detected multiple systems range from 0.21 to 0.96. The detections and derived quantities of each system are listed in Table 4.

Table 4
Physical Separation in au, Masses ($M_\odot$), and Mass Ratios (q)

Target Name (1)	Physical Sep. (au) (2)	M_{prim} ($M_\odot$) (3)	M_{sec} ($M_\odot$) (4)	q (5)
HD 5448	2.760 ± 0.013	2.39	0.60	0.25
HD 11636	1.145 ± 0.013	2.01	1.05	0.52
HD 28910[a]	0.288 ± 0.002	2.21	2.12	0.96
HD 29388	0.480 ± 0.012	2.17	0.67	0.31
HD 48097	1.23 ± 0.04	1.94	0.40	0.21

Note. Companion masses are estimated using the MIST evolutionary models and the assumed primary mass and age from De Rosa et al. (2014); see Table 1.
[a] Mass may be overestimated due to a high mass ratio and prior method of estimation. Mass ratios are still reliable; cf. other A8V stars in sample.

3.2. Detection Limits

CANDID offers a feature that derives the detection limit to any particular target. This is accomplished by injecting artificial companions at particular positions with specific flux ratios and evaluating the significance of a binary fit with those given values. The code then identifies the flux ratio at each step in separation where the significance level is equal to 5σ. Because it searches the entire field of view, any given separation would have many injected companions at many position angles. To determine the detection limit at any given separation without position angle bias, we take the highest flux ratio that returns the 5σ result. In this case, there could be fainter companions at other position angles that correspond to the 5σ limit. This process results in a flux ratio at all steps in separation in which we can recover companions. For targets with detected companions, CANDID also offers the ability to remove the signal of the detection and then carry out the detection limit procedure on the edited data. For sources with detected companions, we defined companion parameters by fitting the closure phase and visibility data for all free parameters, removed the signal, and then performed the detection limits procedure on the residual closure phase data.

Achievable contrasts typically range from $\Delta H = 4.0$ to 5.5 mag beyond $\sim$10 mas. The H-band magnitude of our targets ranges from 2.43 to 6.39 mag. For targets with $H \lesssim 5.8$ mag, we can achieve typical contrasts under good conditions. For targets with $H \gtrsim 5.8$ mag, the achievable contrast is <4 mag at 10 mas, especially with worse weather conditions. In Figure 1, we show the detection limits for each source in our sample with the median value at each separation highlighted in red and the values of the detections represented by red circles. In Table 5, the attainable contrast at select angular separations is given for each source within the sample.

Using the achievable contrast at a given separation, we can calculate the lowest mass of a detectable companion for each target as a function of separation. Given the age (ranging from 10 to 790 Myr) and mass of the primary from De Rosa et al. (2014), we use the MIST evolutionary models to estimate the lowest mass of a detectable companion and the lowest mass ratio of a detectable multiple system at each separation.

Four targets stand out as having poor sensitivity (higher mass ratio limits) relative to the rest of the sample. All four were observed on UT 2020 December 20, the night with poorer observing conditions. Three of the four are the faintest sources in our sample and have H-band $\geqslant$ 5.9 mag (HD 77660, HD 24809, and HD 112734). The other source (HD 115271) was observed at the end of the first night during sunrise, resulting in poor-quality data.

Table 5
Detection Limits (Contrast in Units of Magnitudes for the H Band) Derived for Each Target Using MIRC-X at 1.0, 3.0, 5.0, 10.0, 50.0, and 300.0 mas in Angular Separation

Target Name	[mas] 1.0	3.0	5.0	10.0	50.0	300.0
HD 5448[a]	4.80	4.80	5.01	5.49	5.71	5.06
HD 11636[a]	5.27	5.39	5.40	5.67	5.67	4.02
HD 15550	3.74	4.08	4.22	4.43	4.82	4.19
HD 20677	3.97	3.98	4.25	4.77	5.03	4.44
HD 21912	3.72	3.75	4.14	4.56	4.88	4.05
HD 24809	0.98	1.54	1.99	2.37	2.71	2.02
HD 28910[a]	3.73	4.10	4.20	4.48	5.09	4.28
HD 29388[a]	4.14	5.15	5.47	5.49	5.70	5.34
HD 31647	3.44	4.55	4.59	5.04	5.40	4.80
HD 32301	5.03	5.03	5.22	5.55	5.94	5.48
HD 46089	2.72	3.32	3.66	3.93	4.46	3.90
HD 48097[a]	2.91	3.10	3.61	3.66	4.10	3.48
HD 56537	4.82	5.20	5.44	5.50	5.82	5.50
HD 59037	3.92	4.16	4.37	4.66	4.93	4.36
HD 66664	3.39	4.53	4.74	4.99	5.43	4.88
HD 74198	4.87	4.95	5.38	5.63	5.83	5.46
HD 74873	3.00	4.08	4.23	4.62	5.06	4.47
HD 77660	1.33	1.76	2.28	2.60	2.99	2.37
HD 84107	3.15	3.15	3.48	4.02	4.33	3.73
HD 92941	3.80	4.12	4.39	4.58	4.92	4.26
HD 97244	3.66	3.66	3.92	4.28	4.67	4.05
HD 99787	3.87	3.97	4.16	4.65	4.98	4.19
HD 106661	4.74	4.83	5.01	5.26	5.59	5.03
HD 112734	0.54	0.54	1.01	1.26	1.61	0.81
HD 115271	2.90	3.03	3.29	3.39	3.96	3.46
HD 120047	4.00	4.00	4.23	4.96	5.23	4.58
HD 121164	3.99	3.99	4.37	4.69	5.20	4.56

Note. We define the detection limit as the highest flux ratio companion that CANDID can recover at a given radius that is equivalent to a 5σ detection, with the subsequent injection and recovery procedure.
[a] Binary detections. Limits derived after removal of companion from data.

One target (HD 31647) was observed with both MIRC-X and MYSTIC using five telescopes (instead of all six) with 15 minutes total integration time. Object HD 31647 has $H = 4.98$ mag, a typical brightness for our sample, and we are able to detect companions at the 5σ level down to a contrast of 5 mag beyond 10 mas with both MIRC-X and MYSTIC. The achievable contrast was similar between both instruments, as shown in Figure 2, but slightly better for MYSTIC.

3.3. Binary Population Analysis

Out of 27 A-type stars observed at CHARA, we detected five companions. We must take into account our sensitivity to companions for each source in terms of flux ratio and separation in order to adequately characterize this stellar population.

We first identify a region of common sensitivity in terms of projected separation and mass ratio for the vast majority of our sample that incorporates as many of our detections as possible. We can detect companions down to mass ratios of 0.25 at projected separations of 0.288 au for 20 of the 27 targets in our sample. One target (HD 28910) has a bright companion detection where the signal removal process in CANDID cannot adequately remove all companion features. The achievable mass ratio at the location of the companion is underestimated,

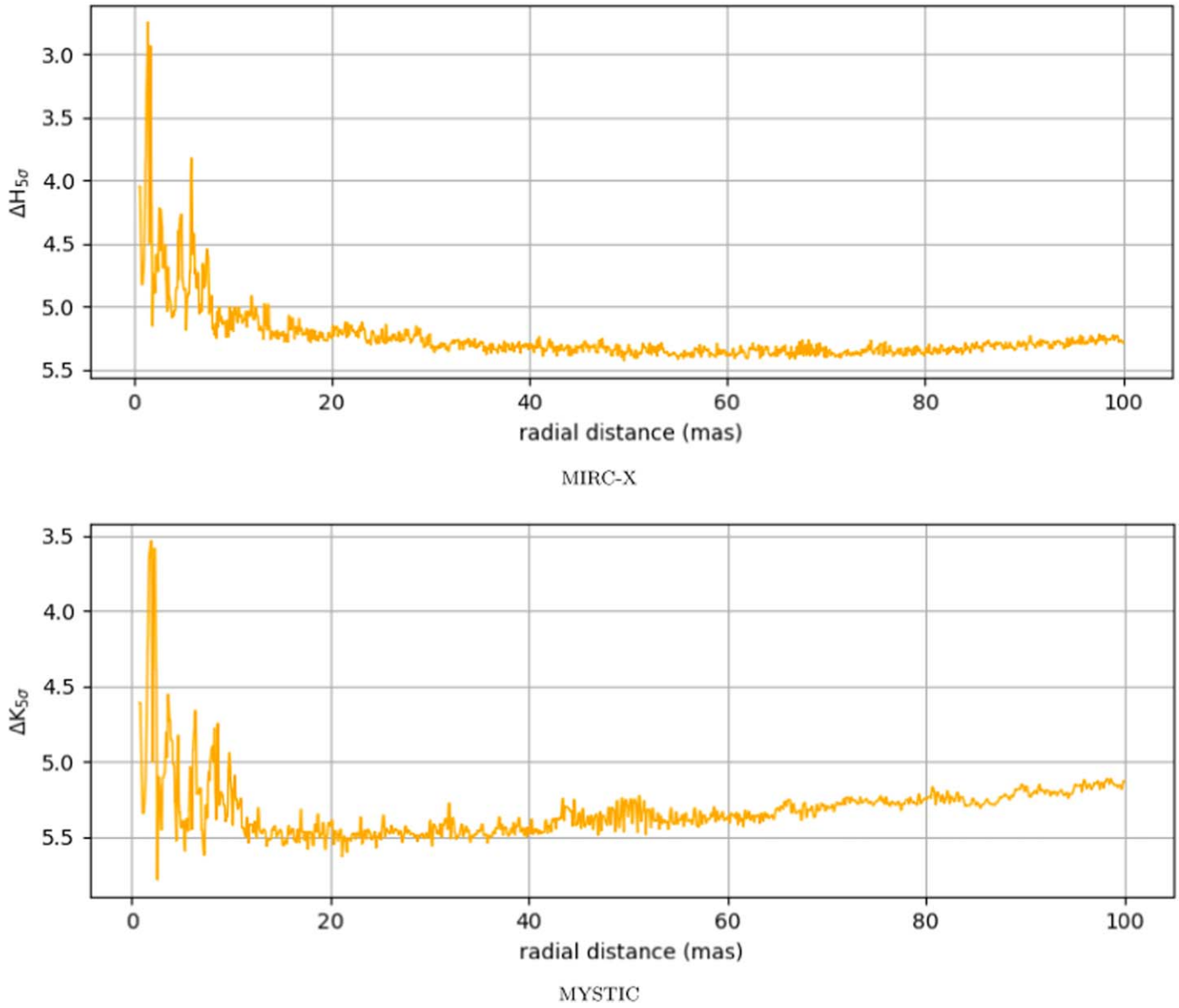

Figure 2. Derived detection limit for HD 31647 as a function of radius from the central star on both the MIRC-X and MYSTIC instruments. These data were collected simultaneously with 15 minute integrations.

while those at locations away from the companion reach the mass ratio of common sensitivity. Therefore, we include this one as having sufficient sensitivity due to both its S/N relative to the rest of the sample and reaching the mass ratio of 0.25 at closer and wider separations. This results in 21 out of 27 targets sensitive to mass ratios $\geqslant$0.25 at separations $\geqslant$0.288 au.

We must also define the common outer working angle of our sample due to the difference in distances as defined in the Gaia archive (Gaia Collaboration et al. 2016, 2021; Babusiaux et al. 2022). For the sake of retaining as many detections and including as many targets as possible in this subsample, we set the outer boundary of our common sensitivity to 5.481 au, the largest detectable companion separation for HD 11636 due to its proximity to the Sun (18.27 pc). Therefore, we require the sensitivity to companions down to mass ratios of 0.25 at separations of 0.288–5.481 au in order to be included in this subsample. We find that for these 21 A-type stars ($M = 1.44$–2.49 $M_{\odot}$) in our sample, there are four detections, resulting in a companion frequency of $0.19^{+0.11}_{-0.06}$ over mass ratios of 0.25–1.0 and projected separations of 0.288–5.481 au. Error bars are derived using the binomial distribution formalism of Burgasser et al. (2003) appropriate for our small sample.

4. Discussion

Our source list was derived from the De Rosa et al. (2014) VAST sample. We excluded sources with known Ap or Am spectral types but did not make sample selections based on previously detected companions. Sources were then randomly selected based on the nights allocated. Of the five binary detections we made over separations of 0.288–2.760 au, three of the sources were targeted for companion search through AO imaging and common proper-motion analysis. They did not find companions to those three over the separations sampled, and they are not known to be triple systems. Object HD 5448 was observed from 32 to 794 and 3980 to 45,000 au, HD 11636

was observed from 32 to 158 and 3980 to 45,000 au, and HD 48097 was observed from 70 to 354 and 1780 to 45,000 au.

4.1. Comparing the Mass Ratios to Models

We cannot place meaningful constraints on the mass ratio distribution of our own sample because we only have five detections, and model fitting suffers from small number statistics. Interestingly, Moe & Di Stefano (2017) and El-Badry et al. (2019) both described a model of the companion population to A stars as weighted toward smaller mass ratios with an excess twin binary component, analyzing results for wider companions from De Rosa et al. (2014). Although we only have five detections, four of those five are smaller mass ratios in the range $q = 0.21$–0.52, where one ($q = 0.96$) is considered a twin ($q \geqslant 0.95$).

Even with a small number of detections, we can compare models of the mass ratio distribution to our sample through the Kolmogorov–Smirnov (K-S) test. The De Rosa et al. (2014) multiplicity survey of A-type stars is sensitive to companions beyond ∼30 au and mass ratios ⩾0.15 for a majority of their sample and describes the mass ratio distribution as a power law for $q \geqslant 0.15$:

$$\frac{dN_1}{dq} \propto q^{\beta}. \tag{1}$$

For companions between 30–125 and 125–800 au, the best fit to the mass ratio distribution has a power-law index $\beta = -0.5^{+1.2}_{-1.0}$ and $-2.3^{+1.0}_{-0.9}$, respectively. Over mass ratios 0.25–1.0, we cannot reject the null hypothesis that our four detections (excluding one with $q = 0.21$ due to being outside the sensitivity of the subsample) are drawn from the same parent population as the distribution of inner ($\beta = -0.5$) or outer ($\beta = -2.3$) binaries from De Rosa et al. (2014) with a K-S test p-value = 0.48 and 0.77, respectively, where a larger sample size is needed to make such a distinction.

4.2. Companion Frequency Comparison

Previous surveys have estimated the companion frequency to A-type stars with methods other than long-baseline interferometry. Murphy et al. (2018) used a phase modulation technique on Kepler light curves (see Murphy et al. 2014) to identify companions to δ Scuti variable stars (type A/F stars). With these data, they are sensitive to companions with periods $\gtrsim$100 days, where incompleteness becomes large, and <1500 days, or ∼0.6–3.6 au. They found a companion frequency of 0.139 ± 0.021 after accounting for white dwarf companions (evolved higher-mass stars that would have served as the primary before evolution). Roughly two-thirds of their companions have $q > 0.25$ after accounting for incompleteness, for a companion frequency of $\sim 0.095 \pm 0.021$. For our sample over $a = 0.6$–3.6 au (the sensitivity of Murphy et al. 2018) and $q \geqslant 0.25$, we detected two companions out of the 21 sources in our subsample for a companion frequency of $0.1^{+0.1}_{-0.03}$, consistent with their results.

Abt (1965) searched for companions to A-type stars using radial velocity measurements from many different publications. It is difficult to constrain the sensitivity of this program (i.e., mass ratio limits) due to undefined errors in some of the measured velocities from past observations. However, they gave a measurement error of ∼2 km s^{-1} for their own measurements, meaning they should be sensitive to stellar companions to intermediate-mass stars from periods of roughly 100–1500 days, the sensitivity of Murphy et al. (2018). Nine of their detections have measured periods between 100 and 1500 days for a companion frequency of $0.16^{+0.06}_{-0.04}$ or $0.13^{+0.06}_{-0.04}$ after accounting for expected white dwarf companions (21% of expected companions). These results are consistent with both the Murphy et al. (2018) results and our own.

Additionally, our survey is sensitive over a defined range of orbital separations and mass ratios that may not correspond to the same sensitivity of previous surveys. However, many large surveys have modeled the distribution of the orbital separations and mass ratios of their companion population using functional forms. We can take those functions and integrate them over the sensitivity of our survey to derive an expected companion frequency of the model over our sensitivity. Then, we can derive a probability that our observations can be described by this model and determine whether the model is representative of our results. We use the models for the companion population to solar-type (Raghavan et al. 2010), A-type (De Rosa et al. 2014), and B-type (Rizzuto et al. 2013) primaries to determine if any may be consistent with our results.

The mass ratio distribution is well fit with a power law (see Equation (1)), and the orbital separation distribution is well fit with a lognormal distribution with a peak ($\log(a_o)$) and width ($\sigma_{\log a}$):

$$\frac{dN_2}{da} = \frac{1}{\sqrt{2\sigma^2_{\log a}}} e^{-\frac{(\log(a)-\log(a_O))^2}{2\sigma^2_{\log a}}}. \tag{2}$$

Integrating the mass ratio distribution of Equation (1) and the orbital separation distribution of Equation (2), we can calculate the expected companion frequency over specified separations and mass ratios assuming they are independent, as shown in De Furio et al. (2019, 2022):

$$\mathrm{CF} = C_n^* \int_{q_1}^{q_2} \frac{dN_1}{dq} \int_{a_1}^{a_2} \frac{dN_2}{da}. \tag{3}$$

First, we solve for C_n by sampling from the companion distribution parameter values of each survey (see Table 6) 10^5 times, assuming Gaussian errors and integrating over the stated sensitivities. Then, we use the value of the constant to calculate the expected companion frequency assuming those companion parameters over the sensitivity of our sample, $q = 0.25$–1.0 and $a = 0.288$–5.481 au. We integrate the binomial distribution of the results of our A-star survey, four detections out of 21 targets, from zero to the companion frequency of each sampling stated above. We then take the mean of these samples to arrive at a posterior probability that this model can describe our observations of A stars over $q = 0.25$–1.0 and $a = 0.288$–5.481 au.

The expected companion frequencies are summarized in Figure 3, where they are presented according to the individual survey. As shown in Table 6, the estimated posterior probabilities for the companion population models to solar-, A-, and B-type primaries are 0.08, 10^{-6}, and 0.46, respectively. These results allow us to conclude that (a) there is a significant population of close companions to A-type stars that must be modeled to have a complete picture of the companion population to intermediate-mass stars, and (b) we find no evidence for a difference between the multiple population of our A-type sample and that of either solar- or B-type stars.

Table 6
Companion Population Parameters and Sensitivities of Each Tested Model with the Resulting Statistics

Primary Spectral Type	β	$\log(a_o)$	$\sigma_{\log a}$	Companion Frequency	$\log(a)$ Sensitivity	q Sensitivity	Expected Companion Frequency	Posterior Probability
FGK type[a]	0	1.7	1.68	0.58 ± 0.02	$-2 \leqslant \log(a) \leqslant 4$	$q \geqslant 0.1$	0.108 ± 0.002	0.08
A type[b]	$-0.5^{+1.2}_{-1.0}$	2.59 ± 0.13	0.79 ± 0.12	0.219 ± 0.026	$1.5 \leqslant \log(a) \leqslant 2.9$	$q \geqslant 0.1$	$0.002^{+0.004}_{-0.0015}$	10^{-6}
A type[b]	$-0.5^{+1.2}_{-1.0}$	2.59 ± 0.13	0.79 ± 0.12	0.338 ± 0.026	$1.5 \leqslant \log(a) \leqslant 4.0$	$q \geqslant 0.1$	$0.002^{+0.004}_{-0.0015}$	10^{-6}
B type[c]	-0.46 ± 0.14	1.05 ± 0.2	1.35 ± 0.2	1.35 ± 0.20	$-2 \leqslant \log(a) \leqslant 4$	$q \geqslant 0.1$	$0.20^{+0.06}_{-0.05}$	0.46

References.
[a] Raghavan et al. (2010).
[b] De Rosa et al. (2014).
[c] Rizzuto et al. (2013).

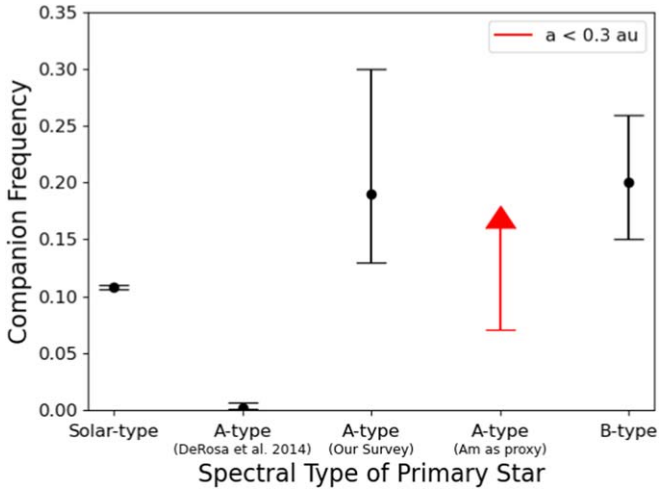

Figure 3. Companion frequencies based on spectral type of the primary star from the various models listed in Section 4.2. All frequencies are calculated over mass ratios = 0.25–1.0 and separations (a) = 0.288–5.481 au, except for Am stars, which were calculated for <0.3 au; see Section 4.3. The companion frequency for solar-type primaries is derived from the model of Raghavan et al. (2010), A-type primaries from the model of De Rosa et al. (2014) and this survey, A-type primaries using Am stars from Carquillat & Prieur (2007), and B-type primaries from the model of Rizzuto et al. (2013).

It is important to note that Moe & Di Stefano (2017) refuted the decrease of the separation distribution of De Rosa et al. (2014) for A-type primaries for <100 au. They argued that this decrease is due to incompleteness for q <0.2 and calculated a consistent companion frequency per decadal bin in the log of the orbital period across roughly $a = 20$–50 and 50–450 au, consistent with flat in log-period space. De Rosa et al. (2014) argued that their model of the orbital separation distribution is inconsistent with the detected companions through radial velocity measurements of Abt (1965) and stated that further observations are required to define the close companion population.

4.3. Comparison to Radial Velocity Survey of Am Stars

Abt & Levy (1985) hypothesized that the Am star (chemically peculiar and slowly rotating) phenomena are the result of a close companion causing tidal braking, which slows the rotation of normal A stars. Once the rotation decreases below ∼100 km s^{-1}, diffusion within the star is allowed to bring metals to the surface, which produces the metallic lines seen in Am stars (Michaud 1980; Michaud et al. 1983). However, not all Am stars appear to have close companions, and the presence of metallic lines may need to be explained without tidal braking. One hypothesis is that as the star evolves off the main sequence, its expansion will slow down the rotation rate (Abt & Levy 1985) below 100 km s^{-1}, allowing diffusion to proceed, producing the metallic lines seen in the Am spectra. Other hypotheses, such as accretion of interstellar material by distorted magnetic fields (Bohm-Vitense 2006), could also explain the presence of higher metal abundances.

Estimates for the occurrence of Am stars among all A-type stars range from 15% to 35% (Bohm-Vitense 2006; Gray et al. 2016; Hummerich et al. 2017; Qin et al. 2019). Based on the results of Carquillat & Prieur (2007), 47% of their Am star sample has companions with periods <30 days (∼0.3 au for an equal-mass binary of 2 $M_\odot$ stars, comparable to our smallest separation detection). If all A-type stars with very close companions become Am stars, then the binary frequency of Am stars at close separations can serve as a proxy for the binary frequency of all A-type stars at those same close separations. Given the fraction of Am stars to all A-type stars (15%–35%) and the binary frequency of Am stars on short orbits (47%; Carquillat & Prieur 2007), we can expect that 7%–16% of all A-type stars have companions with periods <30 days (∼0.3 au); see Figure 3. This result is consistent with our observed companion frequency of $0.19^{+0.11}_{-0.06}$ beyond 0.288 au, indicating that the binary frequency of A-type stars at separations <0.3 au may be comparable to that between 0.288 and 5.481 au.

4.4. Implications

Our analysis of 27 A-type stars within 80 pc observed with long-baseline interferometry reveals a companion frequency of $0.19^{+0.11}_{-0.06}$ over mass ratios of 0.25–1.0 and projected separations of 0.288–5.481 au. In comparison to other multiplicity studies of stellar populations, we find that an extrapolation of the fitted companion properties to the A-type primaries of De Rosa et al. (2014) cannot reproduce the observed companion frequency of our A-star survey over our sensitivity. However, they stated that their model is inconsistent with previous detections at close separations, and further investigations are required to define the companion population at small separations. We could not rule out their best-fit mass ratio distribution (Equation (1)) for either outer ($\beta = -2.3$) or inner ($\beta = -0.5$) binaries based on our results. We do not find any strong statistical differences between the companion frequency of B-type stars in Sco-Cen (Rizzuto et al. 2013) and our sample of A-type stars, nor between that of solar-type stars in the field (Raghavan et al. 2010) and our sample of A-type stars, over the common mass ratios and separations sampled. We also do not find any statistical differences between the very close (<0.3 au) companion frequency of Am stars and the companion frequency of normal A-type stars over our sensitivity. These companion frequencies are summarized in Table 6 and Figure 3, where they are presented according to the individual survey.

It is important to note that all five companions were found at separations between 0.288 and 2.760 au. For many sources in our sample, our survey was sensitive to companions at separations greater than 2.760 au due to their distance (up to 78 pc) and our ability to detect companions out to 0.″3, yet none were found. It is a potentially curious observation, and a larger survey would allow us to probe whether this deficit of companions beyond 2.760 au is statistically significant.

Companions formed through turbulent fragmentation (Goodwin et al. 2004; Offner et al. 2010) are thought to originate at separations of hundreds to thousands of au, while companions formed through disk fragmentation (Adams et al. 1989; Bonnell & Bate 1994; Kratter et al. 2008) are thought to originate at separations on the order of the size of the disk, tens to hundreds of au. Various processes can reduce the separation of the companion below 10 au (Bate et al. 2003; Bate 2012). These processes include accretion from the natal cloud, interactions with the circumbinary disk and gas in the natal cloud, dynamical effects within an unstable triple, the Kozai–Lidov mechanism, and more (Offner et al. 2010; Kratter 2011; Moe & Kratter 2018; Lee et al. 2019; Tokovinin & Moe 2020). We cannot specifically determine which processes affected the binaries observed in our sample. However, we can conclude that

these processes are important to a significant portion of the A-star population and are required to replicate our observations. Although our results do not place strong constraints on the companion population to intermediate-mass A-type stars, they indicate that such a population is significant and must be precisely characterized for a global understanding of star formation processes to intermediate-mass stars. A larger sample size is required, which will enable us to (a) place strong constraints on the companion frequency to A-type stars at close separations, (b) fit various mass ratio distributions for a larger set of companions, and (c) probe the functional form of the close companion orbital separation distribution.

5. Conclusion

We have conducted a survey of 27 nearby A-type stars within 80 pc using long-baseline interferometry at the CHARA Array with the MIRC-X instrument to search for close companions. The results of our survey are summarized as follows.

(1) We have shown that 20 minute integrations with the grism 190 mode on targets with $H \leqslant 5.8$ mag MIRC-X can achieve contrasts of 4–5.5 mag beyond ∼10 mas and 3–4.5 mag beyond 2 mas. We have also shown that MYSTIC has comparable, if not slightly better, sensitivity to faint companions compared to MIRC-X.

(2) We detected five companions with projected separations of 6–65 mas (0.288–2.76 au) and mass ratios = 0.21–0.96. For our sample of A-type stars with masses of 1.44–2.49 $M_{\odot}$, we observed a companion frequency of $0.19^{+0.11}_{-0.06}$ over mass ratios of 0.25–1.0 and projected separations of 0.288–5.481 au. This measurement is consistent with that of the spectroscopic survey of Abt (1965) and the pulsation timing analysis of Murphy et al. (2018) for AF-type primaries over the separations and mass ratios sampled.

(3) Our estimate of the companion frequency is larger than the calculated companion frequency after extrapolating the model fits of De Rosa et al. (2014) to the sensitivity of our survey with a probability of 10^{-6} that they can describe our observations. However, they stated that further investigations are required to completely characterize the companion population down to small separations that are not included in their analysis.

(4) Our detections are consistent with being drawn from both a flat and negatively weighted mass ratio distribution. A larger sample size is crucial to characterizing the mass ratio distribution of close companions to A-type stars.

This work is based upon observations obtained with the Georgia State University Center for High Angular Resolution Astronomy Array at Mount Wilson Observatory. The CHARA Array is supported by the National Science Foundation under grant Nos. AST-1636624 and AST-2034336. Institutional support has been provided from the GSU College of Arts and Sciences and the GSU Office of the Vice President for Research and Economic Development. Time at the CHARA Array was granted through the NOIRLab community access program (NOIRLab PropID 2020B-0290; PI: M. De Furio). MIRC-X received funding from the European Research Council (ERC) under the European Union's Horizon 2020 research and innovation program (grant No. 639889). J.D.M. acknowledges funding for the development of MIRC-X (NASA-XRP NNX16AD43G, NSF-AST 1909165) and MYSTIC (NSF-ATI 1506540, NSF-AST 1909165). We would like to thank the Jean-Marie Mariotti Center for providing the tools ASPRO2 and SearchCal, used to plan observations, available at http://www.jmmc.fr/aspro. S.K. acknowledges support from an ERC Starting Grant and a Consolidator Grant (grant agreement Nos. 639889 and 101003096). This work has made use of data from the European Space Agency (ESA) mission Gaia (https://www.cosmos.esa.int/gaia), processed by the Gaia Data Processing and Analysis Consortium (DPAC; https://www.cosmos.esa.int/web/gaia/dpac/consortium). Funding for the DPAC has been provided by national institutions, in particular the institutions participating in the Gaia Multilateral Agreement.

ORCID iDs

Matthew De Furio https://orcid.org/0000-0003-1863-4960
Tyler Gardner https://orcid.org/0000-0002-3003-3183
John Monnier https://orcid.org/0000-0002-3380-3307
Michael R. Meyer https://orcid.org/0000-0003-1227-3084
Kaitlin Kratter https://orcid.org/0000-0001-5253-1338
Gail Schaefer https://orcid.org/0000-0001-5415-9189
Narsireddy Anugu https://orcid.org/0000-0002-2208-6541
Claire L. Davies https://orcid.org/0000-0001-9764-2357
Stefan Kraus https://orcid.org/0000-0001-6017-8773
Cyprien Lanthermann https://orcid.org/0000-0001-9745-5834
Jacob Ennis https://orcid.org/0000-0002-1575-4310

References

Abt, H. A. 1965, ApJS, 11, 429
Abt, H. A., & Levy, S. G. 1985, ApJS, 59, 229
Adams, F. C., Ruden, S. P., & Shu, F. H. 1989, ApJ, 347, 959
Anugu, N., Le Bouquin, J.-B., Monnier, J. D., et al. 2020, AJ, 160, 158
Babusiaux, C., Fabricius, C., Khanna, S., et al. 2022, arXiv:2206.05989
Bate, M. R. 2012, MNRAS, 419, 3115
Bate, M. R., Bonnell, I. A., & Bromm, V. 2002, MNRAS, 336, 705
Bate, M. R., Bonnell, I. A., & Bromm, V. 2003, MNRAS, 339, 577
Böhm-Vitense, E. 2006, PASP, 118, 419
Bonnell, I. A., & Bate, M. R. 1994, MNRAS, 269
Borgniet, S., Lagrange, A. M., Meunier, N., et al. 2019, A&A, 621, A87
Bourges, L., Mella, G., Lafrasse, S., et al. 2017, VizieR On-line Data Catalog: II/346
Burgasser, A. J., Kirkpatrick, J. D., Reid, I. N., et al. 2003, ApJ, 586, 512
Carquillat, J. M., & Prieur, J. L. 2007, MNRAS, 380, 1064
Che, X., Monnier, J. D., Zhao, M., et al. 2011, ApJ, 732, 68
Choi, J., Dotter, A., Conroy, C., et al. 2016, ApJ, 823, 102
Cummings, J. D., Kalirai, J. S., Tremblay, P. E., Ramirez-Ruiz, E., & Choi, J. 2018, ApJ, 866, 21
De Furio, M., Meyer, M. R., Reiter, M., et al. 2022, ApJ, 925, 112
De Furio, M., Reiter, M., Meyer, M. R., et al. 2019, ApJ, 886, 95
De Rosa, R. J., Patience, J., Wilson, P. A., et al. 2014, MNRAS, 437, 1216
Dotter, A. 2016, ApJS, 222, 8
Duchene, G., & Kraus, A. 2013, ARA&A, 51, 269
El-Badry, K., Rix, H. W., Tian, H., Duchêne, G., & Moe, M. 2019, MNRAS, 489, 5822
Gaia Collaboration, Arenou, F., & Babusiaux, C. 2022, arXiv:2206.05595
Gaia Collaboration, Brown, A. G. A., Vallenari, A., et al. 2021, A&A, 649, A1
Gaia Collaboration, Prusti, T., de Bruijne, J. H. J., et al. 2016, A&A, 595, A1
Gallenne, A., Mérand, A., Kervella, P., et al. 2015, A&A, 579, A68
Goodwin, S. P., Whitworth, A. P., & Ward-Thompson, D. 2004, A&A, 414, 633
Gravity Collaboration, Karl, M., Pfuhl, O., et al. 2018, A&A, 620, A116
Gray, R. O., Corbally, C. J., Cat, P. D., et al. 2016, AJ, 151, 13
Hümmerich, S., Bernhard, K., Paunzen, E., et al. 2017, MNRAS, 466, 1399
Hip 1997, The HIPPARCOS and TYCHO catalogues. Astrometric and photometric star catalogues derived from the ESA HIPPARCOS Space Astrometry Mission, Vol. 1200 (Noordwijk: ESA Publications)
Janson, M., Hormuth, F., Bergfors, C., et al. 2012, ApJ, 754, 44
Jennison, R. C. 1958, MNRAS, 118, 276
Kervella, P., Arenou, F., Mignard, F., & Thévenin, F. 2019, A&A, 623, A72

Kratter, K. M. 2011, ASP Conf. Ser. 4, Evolution of Compact Binaries, ed. L. Schmidtobreick, M. R. Schreiber, & C. Tappert, (San Francisco, CA: ASP), 447
Kratter, K. M., Matzner, C. D., & Krumholz, M. R. 2008, ApJ, 681, 375
Lee, A. T., Offner, S. S. R., Kratter, K. M., Smullen, R. A., & Li, P. S. 2019, ApJ, 887, 232
Michaud, G. 1980, AJ, 85, 589
Michaud, G., Tarasick, D., Charland, Y., & Pelletier, C. 1983, ApJ, 269, 239
Moe, M., & Di Stefano, R. 2017, ApJS, 230, 15
Moe, M., & Kratter, K. M. 2018, ApJ, 854, 44
Monnier, J. D. 2000, in Principles of Long Baseline Stellar Interferometry, ed. P. R. Lawson, Vol. 203 (Pasadena, CA: California Institute of Technology)
Monnier, J. D., Traub, W. A., Schloerb, F. P., et al. 2004, ApJL, 602, L57
Monnier, J. D., Pedretti, E., Thureau, N., et al. 2006, Proc. SPIE, 6268, 62681P
Monnier, J. D., Che, X., Zhao, M., et al. 2012, ApJL, 761, L3
Monnier, J. D., Le Bouquin, J. B., Anugu, N., et al. 2018, Proc. SPIE, 10701, 1070122
Monnier, J. D., Zhao, M., Pedretti, E., et al. 2007, Sci, 317, 342
Murphy, S. J., Bedding, T. R., Shibahashi, H., Kurtz, D. W., & Kjeldsen, H. 2014, MNRAS, 441, 2515
Murphy, S. J., Moe, M., Kurtz, D. W., et al. 2018, MNRAS, 474, 4322
Offner, S. S. R., Kratter, K. M., Matzner, C. D., Krumholz, M. R., & Klein, R. I. 2010, ApJ, 725, 1485
Paxton, B., Bildsten, L., Dotter, A., et al. 2011, ApJS, 192, 3
Paxton, B., Cantiello, M., Arras, P., et al. 2013, ApJS, 208, 4
Paxton, B., Marchant, P., Schwab, J., et al. 2015, ApJS, 220, 15
Paxton, B., Schwab, J., Bauer, E. B., et al. 2018, ApJS, 234, 34
Pourbaix, D. 2000, A&AS, 145, 215
Qin, L., Luo, A. L., Hou, W., et al. 2019, ApJS, 242, 13
Raghavan, D., McAlister, H. A., Henry, T. J., et al. 2010, ApJS, 190, 1
Reid, I. N., Lewitus, E., Allen, P. R., Cruz, K. L., & Burgasser, A. J. 2006, AJ, 132, 891
Rizzuto, A. C., Ireland, M. J., Robertson, J. G., et al. 2013, MNRAS, 436, 1694
Rogers, A. E. E., Hinteregger, H. F., Whitney, A. R., et al. 1974, ApJ, 193, 293
Sana, H., de Mink, S. E., de Koter, A., et al. 2012, Sci, 337, 444
Swihart, S. J., Garcia, E. V., Stassun, K. G., et al. 2017, AJ, 153, 16
ten Brummelaar, T. A., McAlister, H. A., Ridgway, S. T., et al. 2005, ApJ, 628, 453
Tokovinin, A., & Moe, M. 2020, MNRAS, 491, 5158
Webbink, R. F. 1984, ApJ, 277, 355
Whelan, J., & Iben, I. J. 1973, ApJ, 186, 1007
Winters, J. G., Henry, T. J., Jao, W. C., et al. 2019, AJ, 157, 216
Zhao, M., Monnier, J. D., Pedretti, E., et al. 2009, ApJ, 701, 209